COMMUNICATIONS

Photoelectron imaging spectroscopy of molecular and cluster anions: CS_2^- and $OCS^-(H_2O)_{1,2}$

Eric Surber and Andrei Sanov[a)]
Department of Chemistry, University of Arizona, Tucson, Arizona 85721-0041

(Received 7 January 2002; accepted 14 February 2002)

We report the photoelectron imaging study of molecular and cluster anions CS_2^- and $OCS^-(H_2O)_{1,2}$ at 800, 529, and 400 nm, comparing the results for the hydrated OCS^- cluster ions to CS_2^-. The photoelectron angular distributions are interpreted qualitatively using group theory in the framework of the one-electron, electric-dipole approximations. The energetics of $OCS^-(H_2O)_{1,2}$ are compared to the theoretical predictions. The vertical detachment energies of $OCS^- \cdot H_2O$ and $OCS^-(H_2O)_2$ are determined to be 2.07 ± 0.07 and 2.53 ± 0.07 eV, respectively. An indirect estimate of the adiabatic electron affinity of OCS yields a value of -0.04 eV. © *2002 American Institute of Physics.* [DOI: 10.1063/1.1467916]

Photoelectron imaging affords effective opportunities for the studies of negative ions, complementing photoelectron spectroscopy[1] with a heightened emphasis on the electronic wave functions. The imaging approach has been successfully applied to many neutral systems, for which the simultaneous observation of photoelectron energy spectra and energy-resolved photoelectron angular distributions (PAD) was shown to be instrumental in the studies of chemical structure, as well as time-resolved dynamics.[2,3] However, almost no imaging studies were reported for molecular anions.[4]

We present the first photoelectron imaging study of CS_2^- and $OCS^-(H_2O)_{1,2}$ and take steps towards developing a practical approach to interpreting the photoelectron images for molecular and cluster anions. We show that because of convenient symmetry, the PADs in the case of CS_2^- are easy to interpret, at least qualitatively, providing a starting point for the studies of more complex systems, such as $OCS^-(H_2O)_{1,2}$.

By investigating the hydrated clusters, we also aim to unravel the properties of OCS^-. The adiabatic electron affinity (EA) of OCS has long eluded accurate experimental determination, while the theory predicts that it is slightly negative.[5,6] In accord with this prediction, OCS^- is not formed effectively in our ion source. We are able, however, to study this anion stabilized by intermolecular interactions within small gas-phase clusters, using CS_2^- as a reference point for interpreting the results.

The experiments are carried out with the new negative-ion photoelectron imaging apparatus, consisting of a pulsed ion source and mass-spectrometer, described elsewhere,[6] and a photoelectron imaging assembly.[7] CS_2^- is formed by secondary electron attachment in an electron-impact ionized pulsed supersonic expansion of room-temperature carbon disulfide at ambient vapor pressure seeded in 3 atm of Ar. The hydrated anions of carbonyl sulfide are formed as described previously,[6] using OCS seeded in Ar with trace amount of water.

The electrons detached from mass-selected negative ions are detected in the direction perpendicular to the ion beam, using the imaging method of Chandler and Houston[8] in the velocity-mapping modification of Parker and Eppink.[9] The 40 mm dia. microchannel plate (MCP) detector with a phosphor screen (Burle, Inc.) is mounted at the end of a 15 cm long electron flight tube and monitored using a CCD camera (Roper Scientific). To discriminate against noise, the MCPs are operated in a pulsed-bias mode. The velocity-map focusing was optimized and the electron kinetic energy (eKE) calibration was determined using the atomic photodetachment transitions in I^-.

The experiments are carried out using the amplified Ti:Sapphire-based femtosecond laser system from Spectra Physics (1 mJ, 100 fs pulses). The 800 nm measurements used a portion ($\sim$200 μJ/pulse) of the unfocussed fundamental output. The 529 nm radiation (30–50 μJ/pulse) was generated by sum-frequency mixing the signal output of the optical parametric amplifier with the fundamental radiation. The 400 nm light was generated by frequency-doubling a portion of the fundamental in the Super Tripler femtosecond harmonics generator (Super Optronics, Inc.), giving $\sim$120 μJ/pulse. The 529 and 400 nm beams were mildly focused with a 2 m focal-length lens, positioned 1.3 m before the interaction region. The polarization axis was always parallel to the imaging detector plane.

Figures 1(a)–1(c) show the images obtained in the photodetachment of CS_2^- at 400, 529, and 800 nm, with the laser polarization vertical in the image plane. Figures 1(d)–1(f) display the two-dimensional cuts through the respective three-dimensional velocity distributions, reconstructed from the images using the Abel inversion.[10] The experimental images where transformed using a new fitting procedure developed by Reisler and co-workers.[11] The method relies on the

a)Author to whom correspondence should be addressed.

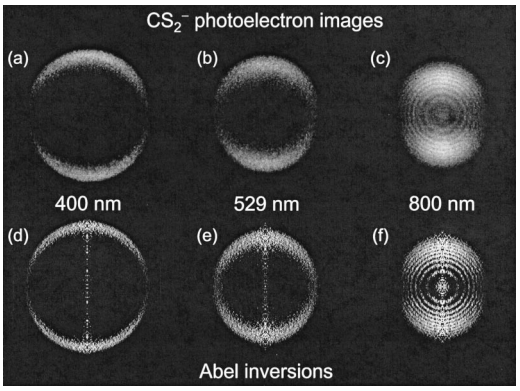

FIG. 1. (a)–(c) Photoelectron images recorded in the photodetachment of CS_2^- at (a) 400, (b) 529, and (c) 800 nm. (d)–(f) Two-dimensional cuts (including the cylindrical symmetry axis) through the respective three-dimensional velocity distributions, reconstructed as described in the text. The images are shown on arbitrary velocity scales (see Fig. 2 for quantitative information). The laser polarization is vertical.

expansion of the raw image with a large basis set of functions that are the analytical Abel transforms of narrow Gaussian functions. The latter constitute the basis set for the reconstructed image.

The images gradually zoom in on the transition structure: the rings corresponding to the vibrational levels of the neutral emerge at 800 nm due to the improved absolute energy resolution at small eKEs. Although the rings are apparent in the raw image in Fig. 1(c), they are most clear in the reconstructed image in Fig. 1(f).

Figure 2(a) shows the photoelectron spectra extracted from the data in Fig. 1. The spectra are plotted versus electron binding energy, $\mathrm{eBE}=h\nu-\mathrm{eKE}$, allowing for direct comparison of all data. The progression of peaks in the 800 nm spectrum is assigned to transitions from the bent ground state of CS_2^- to the excited bending vibrational levels of CS_2, whose equilibrium geometry is linear. The peaks are evenly spaced, with an average spacing of $415\pm10\ \mathrm{cm}^{-1}$, in good agreement with Oakes *et al.*,[12] who observed an average interval of $430\ \mathrm{cm}^{-1}$. Our interval is also consistent with another experimental[13] and a theoretical[5] determinations of the bending vibrational frequency in neutral CS_2 (397 and $408\ \mathrm{cm}^{-1}$, respectively).

An important finding is revealed by examining the energy-dependent PADs. Even the visual examination of the 800 nm images in Figs. 1(c) and 1(f) reveals that the outer vibrational rings are more anisotropic than the inner ones. The values of the anisotropy parameter β,[14] characterizing the PADs within individual rings, are plotted in Fig. 2(b). The increase in β with eKE is attributed to the increasing contribution of higher-l waves, compared to the isotropic s wave dominating the near-threshold detachment.

The observed PADs are understood as follows.[7] Considering the detachment in the molecular frame (MF) within the one-electron, electric-dipole approximations, we require that the direct product of the irreducible representations of the bound and free electron orbitals and the dipole operator is invariant under the symmetry operations of the molecular anion point group (C_{2v}). After determining the allowed symmetries of the free-electron waves, it is convenient to expand

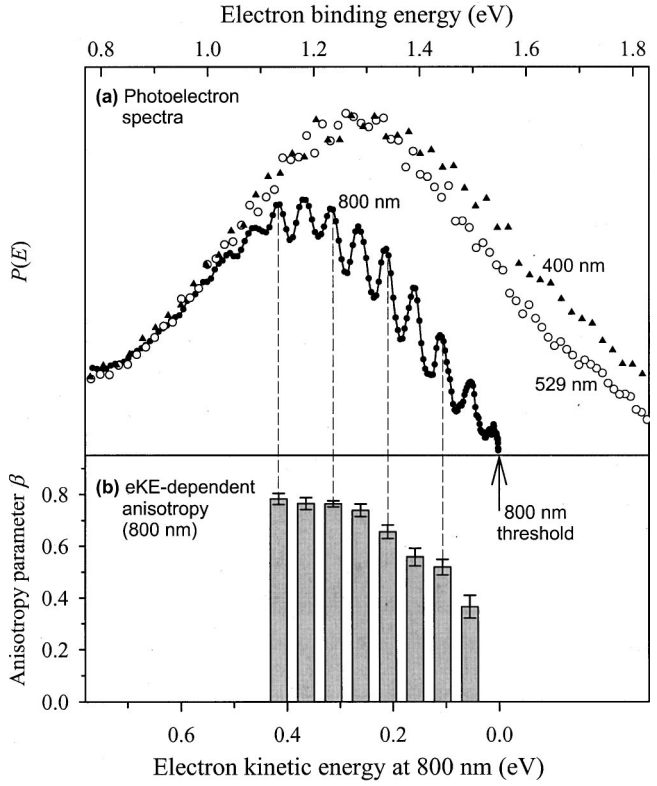

FIG. 2. (a) Photoelectron energy spectra obtained from the CS_2^- images shown in Fig. 1. (b) Energy-dependent anisotropy parameter β, determined by fitting the PADs within the individual vibrational rings in the 800 nm image [Fig. 1(c)].

their angular parts in terms of spherical harmonics. Following the approach of Reed *et al.*,[15] we then make a further approximation (best justified near threshold),[16] considering only the waves with the smallest angular momentum quantum numbers l allowed for each transition.

Since the highest-occupied molecular orbital (HOMO) of CS_2^- is of a_1 symmetry, the detachment transition has the following allowed components (the MF symmetry of the transition dipole moment $\boldsymbol{\mu}$ is given in parentheses):

(a_1) $a_1\rightarrow a_1$, with $\boldsymbol{\mu}_{a_1}\| C_2$, where C_2 is the CS_2^- symmetry axis;

(b_1) $a_1\rightarrow b_1$, with $\boldsymbol{\mu}_{b_1}\perp \mathrm{CS}_2^-$ plane;

(b_2) $a_1\rightarrow b_2$, with $\boldsymbol{\mu}_{b_2}\perp C_2$ within the CS_2^- plane.

The transition amplitude is proportional to the cosine of the angle between the respective $\boldsymbol{\mu}$ (MF-fixed) and the laser polarization axis, denoted here as the laboratory frame (LF) z axis. Setting z to be vertical within the page, the following three types of anion orientations contribute the most to the above transitions:

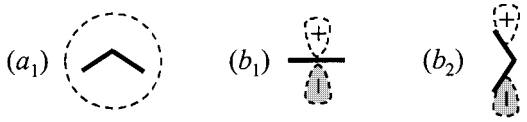

(1)

where the bent frame of CS_2^- is indicated by the bold line [in (b_1), the anion plane $\perp z$], while the meaning of the dashed contours is explained below. The sketched orientations provide optimum alignment of corresponding $\boldsymbol{\mu}$s and contribute the most to the respective transitions. In $(1.a_1)$,

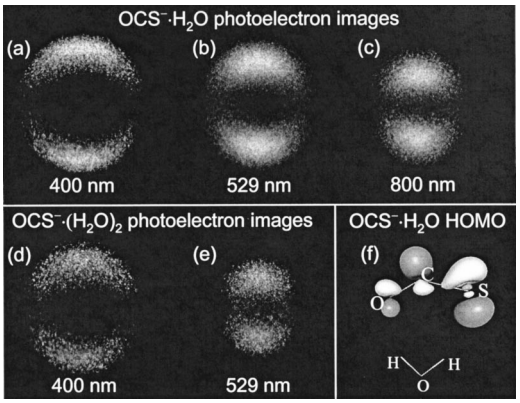

FIG. 3. (a)–(c) Photoelectron images recorded in the photodetachment of $OCS^- \cdot H_2O$ at (a) 400, (b) 529, and (c) 800 nm. (d), (e) photoelectron images of $OCS^-(H_2O)_2$ at 400 and 529 nm, respectively. The images are shown on arbitrary velocity scales (see Fig. 4 for quantitative information). The laser polarization is vertical. (f) The HOMO of the most stable structure of $OCS^- \cdot H_2O$.

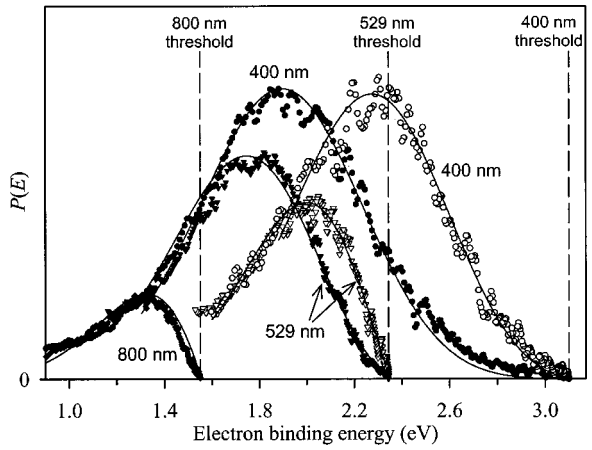

FIG. 4. Filled symbols: Photoelectron energy spectra obtained from the $OCS^- \cdot H_2O$ images in Figs. 3(a)–3(c). Open symbols: photoelectron spectra for $OCS^- \cdot (H_2O)_2$, from Figs. 3(d) and 3(e). Different symbol types correspond to different wavelengths, as labeled. Solid lines: Simulated photoelectron spectra obtained as described in the text, yielding VDE $= 2.07 \pm 0.07$ and 2.53 ± 0.07 eV for $OCS^- \cdot H_2O$ and $OCS^- \cdot (H_2O)_2$, respectively.

$\boldsymbol{\mu}_{a_1} \| z$, while $\boldsymbol{\mu}_{b_1}$, $\boldsymbol{\mu}_{b_2} \perp z$; thus, this orientation yields only a_1 waves. The corresponding smallest-l component is an isotropic s wave, followed by a p_z wave. In $(1.b_1)$, only b_1 waves are produced, with the smallest-l component being a p wave directed along the MF-fixed b_1 axis, which for this orientation coincides with the LF z axis. Finally, in $(1.b_2)$, $\boldsymbol{\mu}_{b_2} \| z$ and the smallest-l wave is also p_z in the LF. The angular properties of the smallest-l waves are indicated in (1) by the dashed contours.

In every case shown in (1), the MF can be rotated about the LF z axis, as well as reflected in the xy plane, giving rise to other orientations yielding the same waves as above. These orientations are, of course, special, as they yield waves of just one symmetry. Quantitative analysis calls for integrating $|\psi|^2$ over all possible orientations, with the free-electron function ψ accounting for the superposition of all allowed waves.

Examining (1), it is noted that the dominant wave contributions are either isotropic or have maximum amplitudes along the laser polarization axis z. Integrating $|\psi|^2$ from these contributions only, yields a PAD peaking along the LF z axis, qualitatively corresponding to $\beta > 0$. All other orientations are intermediate between the above and not expected to change this conclusion.

At small eKEs the cross section for each wave scales approximately in accordance with the Wigner law.[16] Thus, the relative weight of the isotropic s wave is expected to increase for slower electrons, lowering the degree of the anisotropy with decreasing eKE, in agreement with the trend seen in Fig. 2(b).

The 800 nm PAD integrated over all eKEs is characterized by $\beta = 0.68 \pm 0.02$, while the corresponding values derived from the 529 and 400 nm images are 0.73 ± 0.10 and 0.60 ± 0.04, respectively. For the latter two, the energy spectra peak at eKE $= 1.1$ and 1.8 eV, respectively, and the participation of $l > 1$ waves in the detachment process cannot be neglected.

Figures 3(a)–3(c) show the images obtained in the detachment of $OCS^- \cdot H_2O$ at 400, 529, and 800 nm, respectively, while Figs. 3(d) and 3(e) display the images of $OCS^-(H_2O)_2$ at 400 and 529 nm. The weak 800 nm image observed for $OCS^-(H_2O)_2$ is not shown. Compared to CS_2^-, the lack of vibrational ring structure in the $OCS^-(H_2O)_{1,2}$ images is due to the dissociative nature of the cluster ion photodetachment. The anisotropy parameters obtained by fitting the $OCS^- \cdot H_2O$ PADs are practically independent of energy: $\beta = 1.13 \pm 0.06$, 1.20 ± 0.06, and 1.16 ± 0.05 at 400, 529, and 800 nm, respectively. This is probably a consequence of the highly integrated nature on these PADs, arising from a wide energy range and different structural isomers.[6] For $OCS^-(H_2O)_2$, $\beta = 1.06 \pm 0.07$ and 0.99 ± 0.06 at 400 and 529 nm, respectively.

Except for the lack of vibrational rings, the images of $OCS^-(H_2O)_{1,2}$ are overall similar to those of CS_2^-, consistent with the qualitative similarity of the half-filled HOMOs in $OCS^-(H_2O)_{1,2}$ and CS_2^-. The OCS^- and CS_2^- PADs are expected to be similar, as the respective parent orbitals are quite similar. The results thus indicate that one or two water molecules do not alter greatly the OCS^- HOMO. Supporting this conclusion, the calculated HOMO of $OCS^- \cdot H_2O$ is shown in Fig. 3(f).[6]

Since one water molecule does not bind an electron,[17] the $OCS^- \cdot H_2O$ structure of the monohydrated cluster anion is expected. For $[OCS(H_2O)_2]^-$, a water-dimer anionic core is conceivable, but the similarity of the images in Figs. 3(d) and 3(e) to those of $OCS^- \cdot H_2O$ [Figs. 3(a)–3(c)] favors the $OCS^-(H_2O)_2$ structure, in parallel with $CO_2^-(H_2O)_2$.[18]

Additional structural information is revealed by the photoelectron energy spectra shown in Fig. 4. The filled and open symbols represent $OCS^- \cdot H_2O$ and $OCS^- \cdot (H_2O)_2$, respectively, while the different symbol types correspond to different wavelengths, as labeled. The $OCS^- \cdot H_2O$ 400 nm spectrum peaks at 1.87 ± 0.05 eV, in agreement with the VDE of 1.89 eV, predicted for the most stable $OCS^- \cdot H_2O$ isomer, based on CCSD/6-311++G(d,p) calculations.[6] However, the Franck–Condon envelope in the photoelectron spectrum is overlaid with the electronic cross section

σ(eKE), which is why the observed maximum position varies with photon energy, as seen in Fig. 4. Thus, the spectral maximum does not correspond directly to the anion VDE. Accounting for this effect, the solid lines in Fig. 4 indicate the spectra simulated by superimposing the Franck–Condon envelope (assumed Gaussian) with σ(eKE), obtained by modeling the superposition of $l=0$, 1, and 2 waves, disregarding all others.[7] Neglecting the long-range interaction between the electron and neutral $OCS \cdot H_2O$, the scaling of the partial cross sections was approximated by the Wigner law.[16] The consistent modeling of the 400, 529, and 800 nm $OCS^- \cdot H_2O$ photoelectron spectra yields a VDE of 2.07 ± 0.07 eV, which is 0.18 eV larger than the theoretical prediction.

This result has implications for the EA of OCS. At the CCSD/6-311+G(d) level, the adiabatic EA was predicted to be -0.217 eV.[6] Assuming that the coupled-cluster theory underestimates the EA of OCS by the same error as the VDE of $OCS^- \cdot H_2O$, the EA can be estimated as the CCSD prediction (-0.217 eV) plus the 0.18 eV correction based on the measurement of VDE, giving -0.04 eV. This is the first estimate of the evasive, near-zero EA of OCS derived (albeit indirectly) using an experimental measurement. It is in remarkable agreement with the higher-level theoretical prediction of -0.059 ± 0.061 eV obtained using the Gaussian-3 theory.[6]

Modeling the 400 and 529 nm photoelectron spectra of $OCS^-(H_2O)_2$ with the same parameters as above, except for VDE, (solid lines in Fig. 4) yields a VDE value of 2.53 ± 0.07 eV. Thus, the addition of a second water molecule increases the VDE by 0.46 eV, consistent with the 0.52 eV increase in VDE from $CO_2^- \cdot H_2O$ to $CO_2^-(H_2O)_2$,[18] given the larger size of OCS^- compared to CO_2^-.

In summary, we have demonstrated the utility of photoelectron imaging for the studies of molecular and cluster anions on the examples of CS_2^- and $OCS^-(H_2O)_{1,2}$. Since unhydrated OCS^- was not studied directly, the results for $OCS^-(H_2O)_{1,2}$ are compared to CS_2^-. The adiabatic EA of OCS is estimated at -0.04 eV, while the VDEs of $OCS^- \cdot H_2O$ and $OCS^-(H_2O)_2$ are determined to be 2.07 ± 0.07 and 2.53 ± 0.07 eV, respectively. The time-resolved experiments on $(OCS)_n^-$ (now in progress) will probe the metastable OCS^- fragments[19] of cluster dissociation, and provide further insights into the structure and dynamics.

The authors thank W. Carl Lineberger and Hanna Reisler for discussions and comments on the manuscript. Hanna Reisler and Vladimir Dribinski are acknowledged for providing the image analysis software. This work is supported by the NSF instrumentation Grant No. CHE-9982057, the ACS Petroleum Research Fund Grant No. 35589-G6 and the Research Corporation Research Innovation Award No. RI0515.

[1] K. M. Ervin and W. C. Lineberger, in *Advances in Gas Phase Ion Chemistry*, Vol. 1, edited by N. G. Adams and L. M. Babcock (JAI, Greenwich, 1992), p. 121.
[2] L. Wang, H. Kohguchi, and T. Suzuki, Faraday Discuss. **113**, 37 (1999).
[3] J. A. Davies, J. E. LeClaire, R. E. Continetti, and C. C. Hayden, J. Chem. Phys. **111**, 1 (1999).
[4] H. J. Deyerl, L. S. Alconcel, and R. E. Continetti, J. Phys. Chem. A **105**, 552 (2001).
[5] G. L. Gutsev, R. J. Bartlett, and R. N. Compton, J. Chem. Phys. **108**, 6756 (1998).
[6] S. E. Surber, S. P. Ananthavel, and A. Sanov, J. Chem. Phys. **116**, 1920 (2002).
[7] E. Surber and A. Sanov (unpublished).
[8] D. W. Chandler and P. L. Houston, J. Chem. Phys. **87**, 1445 (1987).
[9] A. T. J. B. Eppink and D. H. Parker, Rev. Sci. Instrum. **68**, 3477 (1997).
[10] A. J. R. Heck and D. W. Chandler, Annu. Rev. Phys. Chem. **46**, 335 (1995).
[11] V. Dribinski and H. Reisler (private communication, 2001).
[12] J. M. Oakes and G. B. Ellison, Tetrahedron **42**, 6263 (1986).
[13] I. Suzuki, Bull. Chem. Soc. Jpn. **48**, 1685 (1975).
[14] J. Cooper and R. N. Zare, in *Atomic Collision Processes*, Vol. XI–C, edited by S. Geltman, K. T. Mahanthappa, and W. E. Brittin (Gordon and Breach, New York, 1968), p. 317.
[15] K. J. Reed, A. H. Zimmerman, H. C. Andersen, and J. I. Brauman, J. Chem. Phys. **64**, 1368 (1976).
[16] E. P. Wigner, Phys. Rev. **73**, 1002 (1948).
[17] L. A. Posey, M. J. Deluca, P. J. Campagnola, and M. A. Johnson, J. Phys. Chem. **93**, 1178 (1989).
[18] T. Tsukuda, M. Saeki, R. Kimura, and T. Nagata, J. Chem. Phys. **110**, 7846 (1999).
[19] A. Sanov, S. Nandi, K. D. Jordan, and W. C. Lineberger, J. Chem. Phys. **109**, 1264 (1998).